Parametric pumping of precession modes in ferromagnetic nanodisks

Feng Guo[*]

Center for Nanoscale Science and Technology, National Institute of Standards and Technology, Gaithersburg, Maryland 20899, USA and Maryland Nanocenter, University of Maryland, College Park, MD 20742, USA

L. M. Belova

Department of Materials Science and Engineering, Royal Institute of Technology, 10044 Stockholm, Sweden

R. D. McMichael[†]

Center for Nanoscale Science and Technology, National Institute of Standards and Technology, Gaithersburg, Maryland 20899, USA

We report on the parametric excitation of magnetic precession modes in nanodisks using a parallel pumping configuration. The excitations are detected using a ferromagnetic resonance force microscopy method, and the parallel-pumped spectra reveal nonlinear characteristics including instability thresholds and multiple, narrow, saw-tooth-shaped resonances. These characteristics are in accord with analytical theory and micromagnetic modeling results. Modeled mode profiles of the excitations show that higher order standing spin-wave modes with both even and odd symmetries are excited under parallel pumping.

I. INTRODUCTION

The microwave-frequency dynamics of the magnetization in magnetic nanostructures is qualitatively different from the dynamics in bulk and thin film samples. In bulk and film samples, the dynamics can be conveniently described in terms of plane waves with continuous values for wave vectors. Degeneracy is common in the bulk spin wave spectrum, where many spin waves with different wave vectors may have identical resonance frequencies[1–3]. In contrast, the mode spectrum of a nanomagnet such as a patterned thin film element has only a few discrete modes in a given frequency range, and far less degeneracy. These modes lack the mathematical simplicity of plane waves. Instead, nonuniform fields[4] and boundary conditions[5] for arbitrarily shaped nanomagnets lead to mode profiles that generally defy simple mathematical descriptions[6,8–13].

For bulk and thin film samples, nonlinear phenomena are understood primarily in terms of three types of instability where spin wave modes are parametrically excited[2,3,14]. In the 1st order Suhl instability, the k=0, uniform precession spin wave mode is driven off resonance by a transverse pumping field, and pairs of spin waves are excited parametrically at a frequency equal to half the excitation frequency. This instability process leads to a phenomenon known as subsidiary resonance[15,16]. In the 2nd order Suhl instability, the uniform precession is driven at its resonance frequency and pairs of spin waves are excited that are degenerate with the uniform precession. The experimental signature of this instability is a saturation and broadening of the main resonance peak[15,16]. In both the 1st and 2nd order Suhl instabilities, the spin wave modes gain energy from the uniform precession, which is driven by a transverse pumping field.

Most relevant for this paper, the third instability is a parallel pumping instability where the pumping field is aligned parallel to the equilibrium magnetization direction. Like the 1st order Suhl instability, the driving field frequency is twice the frequency of the excited pairs of spin waves. However, in parallel pumping, the driving field interacts directly with the spin wave modes rather than through the uniform precession mode.[2,3,14] The relationship between precession and excitation frequencies can be interpreted with a scattering picture: a single photon with pumping field frequency $(2f_0)$ and zero momentum splits into two magnons, each having half of the excitation frequency (f_0) and carrying mementum in opposite directions[3,17]. Both energy and momentum are conserved in this scattering process.

The mechanism of parallel pumping can be also understood within a classical picture. With a pumping field parallel to the magnetization vector, no torque is exerted on the magnetization and no precession takes place. However, for a large precession amplitude with an elliptical orbit, such as the one depicted in Fig. 1(a), the z-component of magnetization $\mathbf{M}_z$ oscillates at twice the precession frequency, $2f_0$. As a result, a pumping field oscillating at $2f_0$ can do work, injecting energy into the precession. Both the power injected by the pumping field and the rate of energy loss due to damping are proportional to the sqare of the precession amplitude. Whether the precesson grows or decays depends on whether the pumping field is above or below a critical value.

The parallel pumping phenomenon was first discovered and explained about half century ago[18–20], and it has been observed mostly in either bulk samples and extended films[7,18,19,21–23]. In particular, several nonlinear phenomena based on parallel pumping have been explored in film structures. One example is the parametric amplification of spin-waves and formation of solitons by
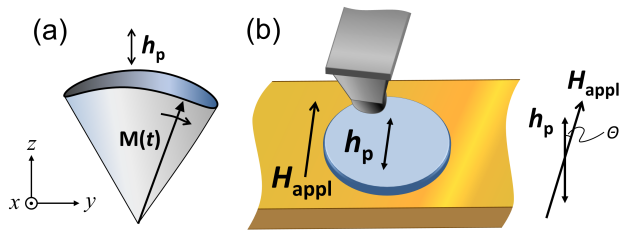
FIG. 1: (Color online) Schematics of (a) magnetization precession in a near-elliptic orbit under a parallel pumping field and (b) experimental setup for ferromagnetic resonance force microscopy.

parallel pumping[24,25]. Another application is the recovery of spin-wave signals via the parametric interaction mechanism[26,27].

More recently, parallel pumping has been investigated in microstructures and nanostructures using Brillouin light scattering spectroscopy. Parametrically excited spin-wave modes have been reported in a 1000 nm × 500 nm Permalloy ellipse[28] and a microstripe[29] with a parallel excitation field. In another work, a single saw-tooth-shaped resonance peak has been observed in a microsize Permalloy disk using parallel pumping, and the instability threshold was found to be tunable by the damping parameter via spin torque effect[30]. Additionally, the parallel pumping phenomenon has also been observed in a thin film with the injection of a radio frequency (rf) pumping current via a nano-point-contact[31–33]. The precession modes associated with parallel pumping were found to be induced by the parallel component of the rf Oersted field.

In this report, we demonstrate parametic excitation of spin-wave modes in a 500 nm diameter $Ni_{80}Fe_{20}$ disk using the parallel pumping geometry. Spectra obtained by parallel pumping are compared to those obtained with transverse pumping. We discuss several nonlinear phenomena observed in the parallel pumping spectra. Analytical theory and micromagnetic modeling show good agreement with experimental results. Size dependent spectra measured in disks with 200 nm, 350 nm and 500 nm diameters are also discussed.

II. METHODS

The samples used in this study have a multilayer structure of Ta (5 nm)/$Ni_{80}Fe_{20}$ (25 nm)/Ta (5 nm). They are patterned into disk shape with diameters ranging from 200 nm to 500 nm using e-beam lithography, e-beam evaporation and a lift-off process. The samples are deposited on a 150 nm thick and 2 μm wide gold waveguide which generates the microwave-frequency pumping field.

The spectra are measured using ferromagnetic resonance force microscopy, which has been developed for detecting magnetization dynamics as well as high resolution magnetic imaging for individual nanostructures[34–39].

In this technique, the precession modes are probed by a cantilever with a magnetic tip made mostly of cobalt, deposited using electron beam induced deposition[40]. The cantilever responds to dipole-dipole like forces between the sample and the tip (Fig. 1(b)), and therefore it measures the reduction in the quasi-static magnetization (ΔM_z) as the ferromagnetic resonance occurs. To improve the signal-noise-ratio, the precession amplitude, and therefore also the tip-sample interaction, are modulated at the mechanical resonance frequency of the cantilever via modulation of the microwave power.

For this study, the cantilever's cobalt tip is about 200 nm in diameter and it is roughly hemispherical in shape.[47] When measuring the spectra, the tip is placed typically 100 nm above the sample, and the applied field is swept with a fixed microwave frequency. The microwave power shown here is the output power from the rf signal generator, when accounting for the total power loss the actual pumping power through the waveguide is much lower than the power of signal generator and is frequency dependent.[48] For convenience, we use decibel (dB) for the unit to indicate the power level relative to 1 mW, i. e., 0 dB of power corresponds to 1 mW. All measurements are done at ambient temperature and under a rough vacuum to enhance the quality factor of the cantilever's mechanical resonance ($Q \approx 10^3$).

The samples are magnetized in-plane by an applied field that can be rotated in the sample plane. For all the measurements shown here, the applied field is oriented at a small angle, $\theta = 20°$, off from the pumping field direction, which allows measuring both parallel and transverse pumping spectra without rotating the applied field. A small transverse component of the pumping field ($h_p \sin\theta$) gives rise to transverse pumping spectra, while the majority of the excitation power is still available for the parallel pumping measurements. In this way, both parallel and transverse pumping spectra can be obtained and compared without rotating the applied field, as we will show in the next section.

III. RESULTS AND DISCUSSION

A. Experimental results

Here we first discuss the measurement results from a 500 nm diameter disk. Within the applied field range (25 mT to 80 mT), a single precession mode is excited at 5.2 GHz by the transverse component of the microwave field, as shown in Fig. 2(a). The spectrum displays a ferromagnetic resonance peak which is Lorentzian in shape, and the inset shows a linear relationship between peak intensity and excitation power level. A linear fit that goes through the origin yields a coefficient of determination (R-squared) of 99.73%. These results are consistent with a linear response for the transverse pumping.

Next, we double the excitation frequency to 10.4 GHz while keeping the field range unchanged. At this fre-
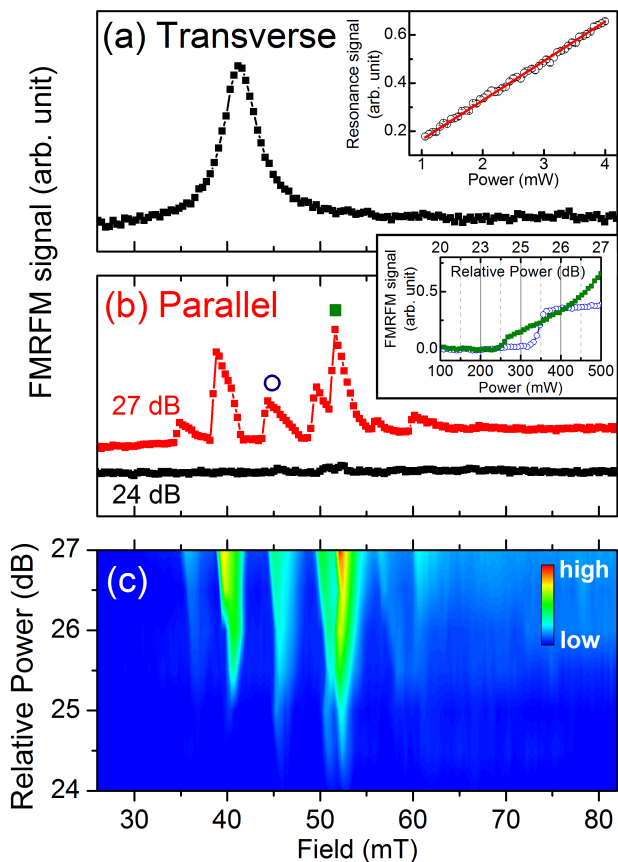
FIG. 2: (Color online) Measured spectra when the microwave frequency is (a) 5.2 GHz at 5 dB for transverse pumping and (b) 10.4 GHz at 27 dB (top) and 24 dB (bottom) for parallel pumping. (c) The power dependent spectra under parallel pumping. The disk is 500 nm in diameter and 25 nm thick. The applied field is 20° off from microwave field direction. The inset in (a) is the resonance peak intensity as a function of microwave pumping power, and the solid line shows the linear fit with a zero intercept. The inset in (b) shows the power dependence of the peak intensities for the two modes labeled in (b). The background signal is measured at an off-resonance field and is subtracted from the data. The power is given in decibels relative to 1 mW.

quency, the transverse component of the rf field is ineffective since it drives the magnetization far from resonance. The longitudinal component, however, provides parametric excitation at twice the precession frequency and it couples to the modes that have elliptical orbits. The parallel pumping spectrum at 27 dB is shown in Fig. 2(b), where it displays several distinct modes. These precession modes show asymmetric peaks with saw-tooth shapes and relatively narrower peak widths compared to the linearly excited resonances.

We now discuss the power dependence in parallel pumping measured from 24 dB to 27 dB. Clear instability threshold behavior is observed: the precession modes do not emerge until certain critical powers, forming the "finger" like structures in the power dependent spectra

in Fig. 2(c). Each "finger" corresponds to a precession mode, and the powers associated with the "fingertips" indicate the critical values for the onset of instability. Furthermore, different modes might have different threshold excitation powers. For example, the mode with resonance field of about 52 mT has the lowest threshold power, while the mode near 46 mT has a slightly higher threshold power. Alternatively, the onset of spin-wave modes can be measured by sweeping the power while fixing the applied field at the modes' resonance fields, as demonstrated in the inset of Fig. 2(b). Two precession modes, labeled with circle and square symbols in the 27 dB spectrum, show critical powers of about 25.1 dB and 24.0 dB respectively.

Thus far, the presented results were obtained with an angle of 20° between the DC applied field and the pumping field. Next, we show that the 10.4 GHz spectra originate from the parallel component of the pumping field. Through the dependence of the spectra on field direction, we find varying the field angle does not alter the main characteristics of the measured spectra. However, the measured resonance fields show a subtle angular dependence. The variation in resonance fields can be up to about 3 mT for $-20° \leq \theta \leq 20°$ and we attribute this to the shape distortion and sample inhomogeneity[39]. Both saw-tooth resonance shape and instability threshold effect are observed within this range of field angle. The peak intensity reduces with increasing angle due to the decreasing parallel field component. For $|\theta| > 25°$, no peaks are found in the 10.4 GHz spectrum at the power level of 25 dB. Although both transverse and parallel components of the pumping field can be simultaneously responsible for parametric excitation (oblique pumping), the angular dependence of the spectra shows the precession modes in Figs. 2(b) and (c) are excited via parallel pumping, even in the presence of a small transverse component of the pumping field.

B. Analytical theory

The instability threshold behavior in parallel pumping can be understood via analytical theory[3]. To describe the motion of a macrospin, we use the Landau-Lifshitz-Gilbert (LLG) equation including a parallel pumping torque term, $-\mu_0 (\mathbf{M} \times \mathbf{h_p})$, where $\mathbf{M}$ is the magnetization vector and $\mathbf{h_p}$ is the oscillating pumping field parallel to the applied field. The equation of motion is linearized under small precession amplitude assumption, and a trial solution, oscillatory with half the frequency of $\mathbf{h_p}$, is introduced. The small-amplitude solution will grow or decay exponentially depending on parameters such as the applied field and the pumping field h_p. The boundary between conditions for growth and decay is given by

$$h_{\mathrm{p}}^{\mathrm{crit}} = P\sqrt{\Delta H_{\mathrm{FWHM}}^2 + 4(H_{\mathrm{appl}} - H_{\mathrm{res}})^2}, \quad (1)$$

where $P = (m_{0,x}^2 + m_{0,y}^2)/|m_{0,x}^2 - m_{0,y}^2|$; $m_{0,x}$ and $m_{0,y}$ stand for oscillation amplitudes of dynamic magnetization in the x and y directions, respectively; ΔH_{FWHM} ($= 2\alpha\omega/(\mu_0\gamma)$, with α being the damping parameter) is the full width at half maximum in linear transverse pumping configuration; H_{appl} is the applied static field; and H_{res} is the resonance field for precession at frequency f_0.

The analytical result reveals three important features of parallel excitation. First, the excitation efficiency is determined by the ellipticity of the precession orbit[23], which is represented by the prefactor $P = (m_{0,x}^2 + m_{0,y}^2)/|m_{0,x}^2 - m_{0,y}^2|$. For a perfectly circular orbit, in which P diverges, precession cannot be parametrically excited. For the samples used in the study, the ratio of diameter to thickness is large (implying a large ratio of demagnetizing factor in x direction to that in y direction) and therefore the ellipticity prefactor is expected to be slightly greater than unity.

Second, $h_{\text{p}}^{\text{crit}}$ also depends on the applied field. The minimum value of $h_{\text{p}}^{\text{crit}}$ is found when the applied field is equal to H_{res}: $h_{\text{p,min}}^{\text{crit}} = P\Delta H_{\text{FWHM}}$, and $h_{\text{p}}^{\text{crit}}$ increases as H_{appl} deviates away from H_{res}. The analytical theory also predicts the peak width for a given microwave power. For example, when the pumping power is 1 dB above the critical value, the predicted full peak width (determined at peak base) is approximately 0.5 ΔH_{FWHM}. The predicted peak width in parallel pumping is qualitatively consistent with the observed narrow peaks in Fig. 2(c) when the pumping power is near the instability threshold.

Third, as mentioned in the introduction section, the instability threshold reflects the balance between the pumping power and energy dissipation due to the damping. The value of $h_{\text{p}}^{\text{crit}}$ reduces with decreasing damping parameter α. This relation explains the observed low critical powers in low damping materials, such as yttrium iron garnet. For a given nonzero ellipticity, the analytical theory predicts a linear dependence of minimum $h_{\text{p}}^{\text{crit}}$ ($H_{\text{appl}} = H_{\text{res}}$) on the damping. This result is consistent with the observed linear relationship between $h_{\text{p}}^{\text{crit}}$ and effective damping[30,31,33].

Finally, we address the saw-tooth shape of the parallel pumped resonances in Fig 2b. For pumping fields larger than the critical value, precession is expected to grow, limited only by some nonlinearity of the system. To find a stable condition at finite amplitude we make the substitution:

$$H_{\text{res}} = H_{\text{res}}^{(0)} - T|a^2| \quad (2)$$

so that H_{res} decreases with the square of precession amplitude a from its low-amplitude value, $H_{\text{res}}^{(0)}$. In transverse pumping measurements at high power (not shown) we observed foldover effects where the resonance shifts toward lower applied fields at higher pumping powers, so we take T to be positive. Alternatively since the time average of M_z also decreases proportionally to the square

of a,

$$H_{\text{res}} = H_{\text{res}}^{(0)} + S\Delta M_z \quad (3)$$

where S has the same sign as T and ΔM_z is strictly negative, since excitation can only reduce M_Z. In the experiment, the force change that we measure is proportional to ΔM_z.

Equation (1) describes the boundary between growing and decaying precession. Previously, we used (1) to determine the grow/decay boundary at small precession amplitudes. Now we use (1) again to find stable solutions at finite amplitudes. Substituting (3) for the amplitude-dependent resonance field and rearranging, (1) yields a stable solution for our measured quantity, $-\Delta M_z$, the quasistatic magnetization change of the sample.

$$-\Delta M_z = \frac{1}{S}\left[H_{\text{res}}^{(0)} - H_{\text{appl}} + \frac{1}{2P}\sqrt{h_{\text{p}}^2 - (h_{\text{p,min}}^{\text{crit}})^2} \right] \quad (4)$$

Equipped with (1) and (4), we are now prepared to describe the line shape. When h_p exceeds the critical value given by (1), small excitations will grow. The resonance field will shift according to (2), and consequently, the growth/decay boundary will also begin to shift. Growth continues until the experimental parameters H_{appl} and h_{p} satisfy (1), and a stable orbit is achieved. The resulting magnetization change given in (4) is found to be a linear function of the applied field, giving the parallel pumped spectra a saw-tooth shape.

C. Micromagnetic modeling

In this section, we present the results of micromagnetic modeling. The analytical approach in the previous section only describes the precession of a single spin. In order to more realistically simulate the parallel pumping in nanomagnets, micromagnetic software, the object oriented micromagnetic framework (OOMMF)[42], is used. The modeled Permalloy-like nanodisk is 500 nm in diameter and 25 nm thick with a cell dimension of $4\times4\times25$ nm^3. For each value of the in-plane applied field, the ground state of the magnetization, such as Fig. 3(d), was calculated using energy minimization.

For a transverse pumping field, the dynamic response to a short field pulse is calculated in the presence of a uniform applied field. Fig. 3(a) shows the calculated susceptibility spectrum under transverse pumping. With a 5.2 GHz pumping frequency, one major precession mode is found. This resonance peak has a Lorentzian shape, similar to the measured spectrum in Fig. 2(a).

For calculating the parallel pumping spectra, the oscillating field was applied parallel to the applied field. After calculating the dynamics for 200 ns to allow a steady state to emerge, the magnetization was recorded for 10 ns, and a time averaged value of the magnetization was then obtained. An example of calculated parallel pumping spectra is shown in Fig. 3(b). In qualitative
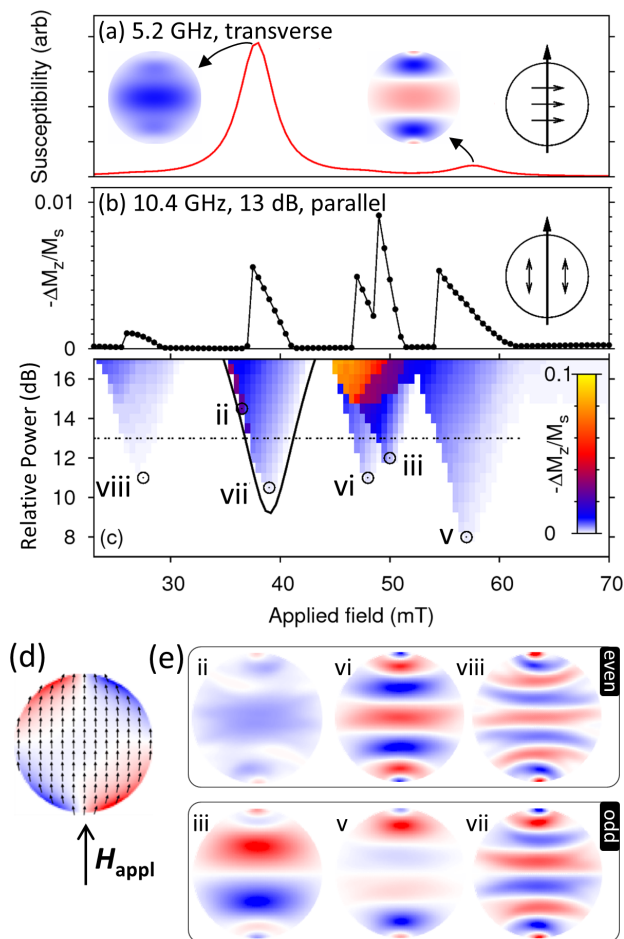
FIG. 3: (Color online) Modeled spectra under (a) transverse pumping (5.2 GHz) and (b) parallel pumping at 13 dB and 10.4 GHz. Insets in (a) are modeled precession mode profiles. (c) Power dependent parallel pumping spectrum. (d) An example of the ground state magnetization configuration under an applied static field. (e) Snapshots of the precessional modes corresponding to the labeled points in (c). The color code in (a), (d) and (e) indicates the transverse component of the magnetization, i. e., blue and red colors represent the left and right components of the magnetization, respectively. The mode indices are based on the number of the nodes.

agreement with experiment results, the modeled parallel pumping spectra also show multiple precession modes which have saw-tooth like peaks with sharp jumps appearing on the low-field sides of the peaks. The peak maximum shifts towards low field with increasing pumping power. In addition, the modeled spectra under parallel pumping is also examined over a broad range of microwave power (9 dB), as plotted in Fig. 3(c). The power dependence reveals features in parallel pumping geometry, including instability threshold behavior as well as the "finger" structures, similar to those in the measurements. Although the measured parallel pumping spectra are qualitatively in good agreement the modeling results, they are not identical. We attribute the discrepancy to the sample distortion and material imperfection caused

by the fabrication, which can affect the measured resonance fields and instability thresholds.

Additionally, representative images of the precession modes were obtained by calculating differences between the recorded magnetization patterns and the ground states. The modeled imaging for parallel pumping is shown in Fig. 3(e). Except for mode "ii", which has a broad distribution nearly across the entire disk, all other modes show standing spin waves, the nodal lines of which are nearly perpendicular to the applied field. An important feature of parallel pumping is that both even-symmetry modes (ii, vi, viii) and odd-symmetry modes (iii, v, viii) are excited. In transverse pumping, however, only modes with an even symmetry, such as those shown in Fig. 3(a), couple to the pumping field, and odd modes are generally not excited. Note that the mode "vii" does not correspond to the uniform center mode, although its resonance field is similar to that of the FMR mode in transverse pumping. The quasi-uniform mode "ii" does not emerge until a higher power of 14 dB.

To compare the analytical expression for the critical pumping field with the modeling results, we use Eq. (1) to compute the field dependent critical power for precession modes. The precession ellipticity factor is obtained from the modeling. The calculated $h_{\mathrm{p}}^{\mathrm{crit}}$ as a function of H_{appl} for mode "vii" is shown in Fig. 3(c). The curve closely matches the contour for mode "vii", showing that the macrospin LLG model captures the parallel pump instability threshold.

D. Size dependence

Parallel pumping allows a more complete view of the mode structure than the typical transversely-pumped ferromagnetic resonance experiment. In this section we exploit this fact to examine the dependence of the mode structure as a function of disk diameter. In addition to the 500 nm diameter disk discussed earlier, 200 nm and 350 nm diameter disks, with the same thickness of 25 nm, are also studied. All these samples are on the same waveguide, spaced 7 μm apart. 10.4 GHz microwave frequency, and power range of 24 dB to 27 dB are used for the measurements.

We point out two trends in the size dependence data shown in Fig. 4. First, as the disk diameter decreases the number of observed modes decreases. When the disk diameter reduces to 350 nm, four modes are observed at 27 dB. Even fewer modes are seen for the 200 nm disk diameter: only one strong mode near 52 mT and two faint modes with higher resonance fields. The size dependent mode number can be interpreted in terms of the finite-size effects. For instance, the spin-wave spectrum is continuous for infinite films, and broad resonances have been observed under parallel pumping[22,43]. For confined systems, however, the corresponding spin-wave dispersion is expected to be discrete due to the quantization of the wave vector[3,44]. In smaller samples, the spin-wave
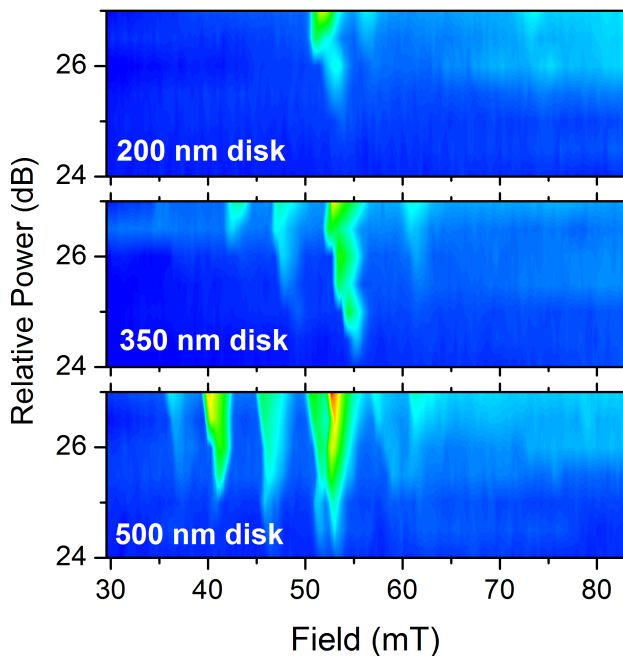
FIG. 4: (Color online) Power dependent spectra under parallel pumping for disk diameters (from top to bottom) 200 nm, 350 nm, and 500 nm. Microwave frequency for all samples are fixed at 10.4 GHz.

spectrum becomes more sparse and generally a simpler spectrum of fewer precession modes is expected[45,46].

The second general trend is that the instability threshold increases with decreasing sample size. The minimum critical power for the 350 nm disk is slightly higher than that for the 500 nm disk, and the critical power for the 200 nm disk is roughly 1 dB higher than the other two disks. This trend can be understood in terms of the size dependent ellipticity. As the disk diameter decreases while the thickness remains constant, the diameter to thickness ratio decreases and the disks trend closer to a spherical shape, where the precession would be circular. Therefore the ellipticity factor reduces for smaller disks. Since the excitation efficiency in parallel pumping

couples to the orbital ellipticity as described earlier in Eq. (1), higher pumping power is required for the onset of instability in smaller samples.

IV. SUMMARY

In summary, we have measured parallel pumping resonances in nanodisks using ferromagnetic resonance microscopy. In contrast to the linearly excited ferromagnetic resonance in transverse pumping geometry, the spin-wave modes in parallel pumping show strong nonlinearities and precess at half of the excitation frequency. The parallel pumping spectra distinguish multiple sawtooth shape resonances in a nanodisk, providing a richer set of resonances than the more conventional transverse pumping. These parametrically excited spin-wave modes exhibit threshold behavior of the instability. An analytical theory and micromagnetic modeling are used to further investigate the parallel pumping, and they display various nonlinear properties consistent with experiment results. The modeling also suggests that spin-wave modes with both even and odd symmetries are excited under parallel pumping. The disk size dependence with constant thickness shows that the critical power for parametric pumping increases with decreasing disk size, and fewer precession modes are observed in smaller structures.

* Electronic address: feng.guo@nist.gov
† Electronic address: robert.mcmichael@nist.gov
1 T. Holstein and H. Primakoff, Phys. Rev. 58, 1098 (1940).
2 M. Chen and C. E. Patton, in *Nonlinear Phenomena and Chaos in Magnetic Materials* (World Scientific, 1994), chap. 3.
3 A. G. Gurevich and G. A. Melkov, *Magnetization Oscillations and Waves* (CRC Press, Inc., 1996).
4 J. Jorzick, S. O. Demokritov, B. Hillebrands, M. Bailleul, C. Fermon, K. Y. Guslienko, A. N. Slavin, D. V. Berkov, and N. L. Gorn, Phys. Rev. Lett. 88, 047204 (2002).
5 K. Y. Guslienko and A. N. Slavin, Phys. Rev. B 72, 014463 (2005).
6 O. Gérardin, H. Le Gall, M. J. Donahue, and N. Vukadin-

iovic, J. Appl. Phys. 89, 7012 (2001).
7 G. Wiese, L. Buxman, P. Kabos, and C. E. Patton, J. Appl. Phys. 75, 1041 (1994).
8 R. D. McMichael and M. D. Stiles, J. Appl. Phys 97, 10J901 (2005).
9 M. Bailleul, R. Höllinger, and C. Fermon, Phys. Rev. B 73, 104424 (2006).
10 C. Bayer, J. Jorzick, B. Hillebrands, S. O. Demokritov, R. Kouba, R. Bozinoski, A. N. Slavin, K. Y. Guslienko, D. V. Berkov, N. L. Gorn, et al., Phys. Rev. B 72, 064427 (2005).
11 V. E. Demidov, U.-H. Hansen, and S. O. Demokritov, Phys. Rev. Lett. 98, 157203 (2007).
12 M. Grimsditch, G. K. Leaf, H. G. Kaper, D. A. Karpeev,

and R. E. Camley, Phys. Rev. B **69**, 174428 (2004).

[13] V. V. Kruglyak, P. S. Keatley, R. J. Hicken, J. R. Childress, and J. A. Katine, J. Appl. Phys. **99**, 08F306 (2006).

[14] H. Suhl, J. Phys. Chem. Solids **1**, 209 (1957).

[15] R. W. Damon, Rev. Mod. Phys. **25**, 239 (1953).

[16] N. Bloembergen and S. Wang, Phys. Rev. **93**, 72 (1954).

[17] V. S. L'vov, *Wave Turbulence Under Parametric Excitation* (Springer-Verlag, 1994).

[18] F. R. Morgenthaler, J. Appl. Phys. **31**, S95 (1960).

[19] E. Schlömann, J. J. Green, and U. Milano, J. Appl. Phys. **31**, S386 (1960).

[20] E. Schlömann, J. H. Saunder, and M. H. Sirvetz, Trans. IRE **MTT 8**, 96 (1960).

[21] W. Wettling, W. D. Wilber, P. Kabos, and C. E. Patton, Phys. Rev. Lett. **51**, 1680 (1983).

[22] C. W. Sandweg, Y. Kajiwara, A. V. Chumak, A. A. Serga, V. I. Vasyuchka, M. B. Jungfleisch, E. Saitoh, and B. Hillebrands, Phys. Rev. Lett. **106**, 216601 (2011).

[23] A. A. Serga, C. W. Sandweg, V. I. Vasyuchka, M. B. Jungfleisch, B. Hillebrands, A. Kreisel, P. Kopietz, and M. P. Kostylev, Phys. Rev. B **86**, 134403 (2012).

[24] A. V. Bagada, G. A. Melkov, A. A. Serga, and A. N. Slavin, Phys. Rev. Lett. **79**, 2137 (1997).

[25] P. A. Kolodin, P. Kabos, C. E. Patton, B. A. Kalinikos, N. G. Kovshikov, and M. P. Kostylev, Phys. Rev. Lett. **80**, 1976 (1998).

[26] A. A. Serga, A. V. Chumak, A. André, G. A. Melkov, A. N. Slavin, S. O. Demokritov, and B. Hillebrands, Phys. Rev. Lett. **99**, 227202 (2007).

[27] G. A. Melkov, Y. V. Koblyanskiy, R. A. Slipets, A. V. Talalaevskij, and A. N. Slavin, Phys. Rev. B **79**, 134411 (2009).

[28] H. Ulrichs, V. E. Demidov, S. O. Demokritov, and S. Urazhdin, Phys. Rev. B **84**, 094401 (2011).

[29] T. Brächer, P. Pirro, B. Obry, B. Leven, A. A. Serga, and B. Hillebrands, Appl. Phys. Lett. **99**, 162501 (2011).

[30] E. R. J. Edwards, H. Ulrichs, V. E. Demidov, S. O. Demokritov, and S. Urazhdin, Phys. Rev. B **86**, 134420 (2012).

[31] S. Urazhdin, V. Tiberkevich, and A. Slavin, Phys. Rev. Lett. **105**, 237204 (2010).

[32] F. Ciubotaru, A. A. Serga, B. Leven, B. Hillebrands, and L. Lopez-Diaz, Phys. Rev. B **84**, 144424 (2011).

[33] H. Schultheiss, X. Janssens, M. van Kampen, F. Ciubotaru, S. J. Hermsdoerfer, B. Obry, A. Laraoui, A. A. Serga, L. Lagae, A. N. Slavin, B. Leven, and B. Hillebrands, Phys. Rev. Lett. **103**, 157202 (2009).

[34] I. Lee, Y. Obukhov, G. Xiang, A. Hauser, F. Yang, P. Banerjee, D. Pelekhov, and P. Hammel, Nature **466**, 845 (2010).

[35] H.-J. Chia, F. Guo, L. M. Belova, and R. D. McMichael, Appl. Phys. Lett. **101**, 042408 (2012).

[36] A. Hamadeh, G. de Loubens, V. V. Naletov, J. Grollier, C. Ulysse, V. Cros, and O. Klein, Phys. Rev. B **85**, 140408 (2012).

[37] H.-J. Chia, F. Guo, L. M. Belova, and R. D. McMichael, Phys. Rev. B **86**, 184406 (2012).

[38] H.-J. Chia, F. Guo, L. M. Belova, and R. D. McMichael, Phys. Rev. Lett. **108**, 087206 (2012).

[39] F. Guo, L. M. Belova, and R. D. McMichael, Phys. Rev. Lett. **110**, 017601 (2013).

[40] L. M. Belova, E. D. Dahlberg, A. Riazanova, J. J. L. Mulders, C. Christophersen, and J. Eckert, Nanotechnology **22**, 145305 (2011).

[41] Y. H. Liu and C. E. Patton, J. Appl. Phys. **53**, 5116 (1982).

[42] M. J. Donahue and D. G. Porter, in *Interagency Report NISTIR 6376* (National Institute of Standards and Technology, Gaithersburg, MD, 1999).

[43] K. Ando and E. Saitoh, Phys. Rev. Lett. **109**, 026602 (2012).

[44] J. Jorzick, S. O. Demokritov, C. Mathieu, B. Hillebrands, B. Bartenlian, C. Chappert, F. Rousseaux, and A. N. Slavin, Phys. Rev. B **60**, 15194 (1999).

[45] J. M. Shaw, T. J. Silva, M. L. Schneider, and R. D. McMichael, Phys Rev B **79**, 184404 (2009).

[46] T. Kaneko, S. M. Noh, K. Miyake, M. Sahashi, and H. Imamura (2012), cond-mat/1202.6464.

[47] The tips stray field, measured from a separate lift-off dependence experiment, is around 2 mT. However, this relatively small tip field does not affect the qualitative shape of the measured spectra.

[48] For this particular waveguide used, the measured overall power loss is approximately -16 dB at 5 GHz and -27 dB at 10 GHz. For example, the RF field amplited at 5 GHz and 24 dBm is estimated to be on the order of magnitude of 1 mT.